

Acceleration from short-duration blast

D. V. Ritzel¹  · S. Van Albert² · V. Sajja³ · J. Long³

Received: 15 March 2017 / Accepted: 22 September 2017 / Published online: 23 October 2017
© Springer-Verlag GmbH Germany (outside the USA) 2017

Abstract The blast-induced motion of spheres has been studied experimentally where the shock wave is rapidly decaying during the period that quasi-steady acceleration would be developed in the case of a step-function shock wave as considered in most shock-tube studies. The motion of sphere models ranging from 39 to 251 mm in diameter and having a range of densities was assessed using the “free-flight” method in a simulator specially designed to replicate the decaying shock wave profile of spherical blast including negative phase and positive entropy gradient. A standardized blast-wave simulation of 125 kPa and 6-ms positive-phase duration was applied for all experiments. In all cases, there are three phases to the motion: a relatively low “kickoff” velocity from the shock diffraction, acceleration or deceleration during the positive duration, then deceleration through the negative phase and subsequent quiescent air. The unexpected deceleration of larger spheres after their kickoff velocity during the decaying yet high-speed flow of the blast wave seems associated with the persistence of a ring vortex on the downstream side of the sphere. The flow is entirely unsteady with initial forces dominated by the shock diffraction; therefore, the early motion of spheres under such conditions is not governed by quasi-steady drag as in classi-

cal aerodynamics. The work will help establish scaling rules for model studies of blast-induced motion relevant to improvised explosive devices, and preliminary results are shown for motion imparted to a human skull surrogate.

Keywords bTBI · Blast simulators · Blast effects · Blast scaling · Blast-induced motion

1 Introduction

Blast-induced motion of unrestrained objects has been studied where the accelerating force is dominated by quasi-steady drag and the imparted velocity scales roughly with dynamic pressure impulse, e.g., [1–3]. However, motion analyses have not been well developed for blast/target scenarios in which the blast wave is decaying rapidly in the same timescale as the early acceleration period in the case of quasi-steady after-flow behind the shock. The period of acceleration after the shock-front passage is sometimes called the “relaxation” regime prior to the accelerating object reaching equilibrium with the post-shock flow [4]. Alternatively, this can be considered with respect to the blast wavelength λ approaching the characteristic length of the structure L which is typical of improvised explosive device (IED) attacks against personnel or vehicles. Scaling criteria for imparted motion is important for the proper interpretation of blast-wave acceleration injuries developed in animal or other model experiments compared to the human case.

The sphere is an important generic shape relevant to a range of shock wave interaction problems, and many experimental and computational studies have been conducted since the 1960s on the matter of shock-wave induced loading or motion of spheres or spherical particles. Prior research tends to fall into four broad categories:

Communicated by O. Petel and S. Ouellet.

✉ D. V. Ritzel
dritz@dyn-fx.com

- ¹ Dyn-FX Consulting Ltd, 19 Laird Ave North, Amherstburg, ON N9V 2T5, Canada
- ² The Geneva Foundation Supporting Walter Reed Army Institute of Research, Walter Reed Army Institute of Research, 503 Robert Grant Drive, Silver Spring, MD 2091-7500, USA
- ³ Walter Reed Army Institute of Research, 503 Robert Grant Drive, Silver Spring, MD 20910-7500, USA

1. Objects such as domed structures ($\sim 1\text{--}10\text{ m}$) loaded by nuclear-scale blast waves, e.g., [5,6]
2. Spheres the scale of powder, dust particles, or beads ($< 10\text{ mm}$) displaced by a step-function shock wave with steady after-flow, e.g., [4,7,8]
3. Intermediate-scale spheres ($\sim 0.01\text{--}0.1\text{ m}$) fixed in a step-function shock wave with steady after-flow to determine net loading force with time and hence unsteady drag coefficient, e.g., [9–13]
4. Intermediate-scale spheres partly restrained in a step-function shock wave with steady after-flow, e.g., [13–15], “partly restrained” refers to any boundary condition for the sphere that would affect the initial shock interaction or motion.

The references cited above are only illustrative examples, and substantially more work has been published in these categories as described in the literature reviews included in [7, 16, 17] for example. Parmar et al. [17] derived an analytic solution for the shock-diffraction phase, although the treatment of the actual shock-reflection process was simplistic. However, in all cases above the loading under consideration is a step-function shock wave with steady after-flow as generated for classical shock-tube studies or a blast wave of very long duration having negligible gradients in the post-shock flow.

With regard to shock waves having decaying after-flow characteristic of free-field explosive blast, the experimental work of [16] did involve a decaying shock wave profile although this was not by design but an artifact of the shock-tube configuration. The problem was treated as quasi-steady accounting for only the relative velocity of particle and freestream flow without consideration of the possible role of the freestream gradients themselves. Furthermore, the early particle motion in that case was highly irregular due to the spherical beads being initially laid on the shock-tube floor, which would strongly affect the shock diffraction and incur artifacts from the shock-tube boundary layer. A computational simulation is described in [18] for the case of various blast profiles on a cylinder comparing inviscid to viscous solutions. However, attention was directed to the flow patterns developed around a fixed cylinder rather than its loading and induced motion. Temkin and Mehta [19] extended earlier experimental work [20] on the acceleration of fine water droplets by a propagating N-wave characteristic of a sonic boom. The shock strengths in those studies were in the acoustic regime, below 0.03 atm, and the droplets around $150\text{ }\mu\text{m}$, entailing very low Reynolds number < 100 . Their primary conclusion was that departure of their results from those for steady drag “cannot be explained in terms of existing theory”, and they speculated the effect was due to changes in the recirculating region behind the sphere, which were related to the gradient in the post-shock flow. To the authors’ knowledge little attention has been directed to the problem of the

motion of a sphere subjected to a decaying blast wave where the positive flow duration is well within the relaxation period expected in the case of a steady after-flow, and where both the diffraction-phase impulse and aerodynamic drag have strong roles. This scenario is relevant to the matter of blast-induced head motion from IED-scale attack and proper scaling of such effects for animal and other model experiments. Several studies addressing the problem of blast-induced traumatic brain injury (bTBI) have suggested violent head accelerations may be imparted under relatively moderate blast loading and may be responsible for brain injury, e.g., [21,22]. However, there are serious questions as to the experiment design exaggerating head-whipping conditions [23] as well as the matter of scaling motion determined from studies with animal models to the human case. There is substantial anecdotal evidence from blast tests with manikins as well as recent technical studies, e.g., [24,25], that suggest that a human head-form incurs negligible motion during the passage of short-duration blast of moderate intensity. Rather than being violently thrown by the effects of the blast dynamic pressure, brain injury may be inflicted by the transient crushing action of the diffracting shock front over the skull.

Although clearly the human head is not spherical and its motion under blast loading will be strongly affected by factors such as the presence of a helmet and its articulation with the neck and body, understanding a sphere’s blast-induced motion provides important guidance regarding the basic phenomenology to be expected. Another important objective of this work is to generate high-quality experimental data for validation of computational simulations. Although highly simplified by the axisymmetric geometry, the motion of a rigid sphere in a blast flow is a state-of-the-art problem of coupled fluid/structure interaction.

Motion induced from a step-function shock wave is considered an unsteady flow problem since the sphere is initially at rest and is accelerated by the uniform shock after-flow. Therefore, the current problem might be considered “doubly” unsteady: the sphere is being accelerated by a rapidly decaying flow having strong pressure, velocity, and entropy gradients.

2 Experimental method

The WRAIR ABS2 shown in Fig. 1 is an Advanced Blast Simulator design [26] having a 60-cm (2 ft.) square test section; a window for the test section allows high-speed video imaging of target response including free-flight motion in this case. The Advanced Blast Simulator technology was critical for the purposes of this study. The ABS2 design is such that the wave dynamics of free-field explosive blast are inherently replicated, generating a positive entropy gradient through the flow and a true negative phase with both under-pressure and

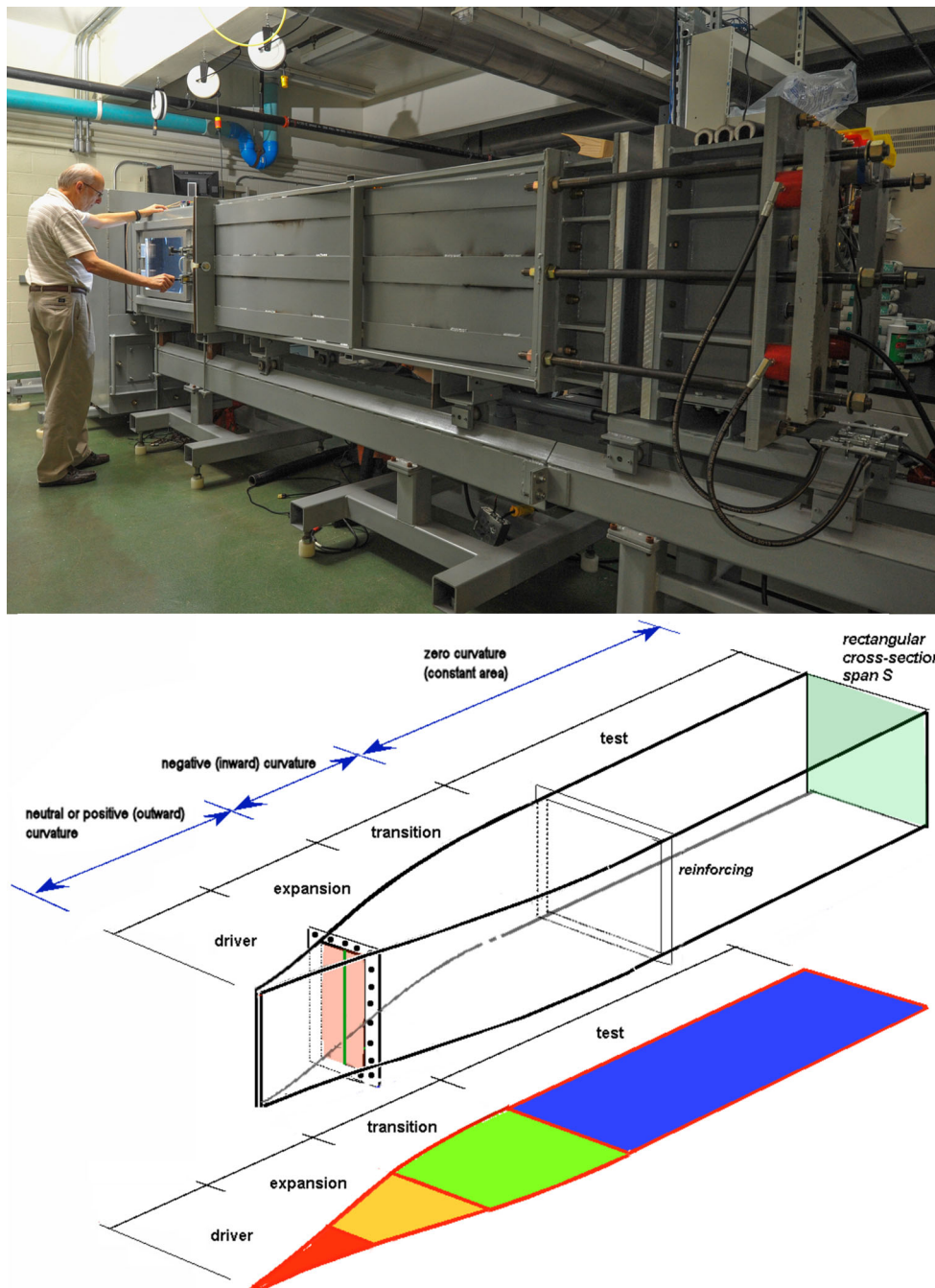


Fig. 1 (Upper) Photograph of the WRAIR ABS2 blast-wave simulator with 60-cm square test section. The compressed-gas driver is shown at right; the test section with imaging window is visible at left; the far end of the simulator includes an end-wave eliminator to preclude anomalous

waves affecting the test section after the shock wave passage. (Lower) Schematic of the ABS2 geometry showing the geometric area expansion from the apex at the closed end of the driver past the diaphragm station

flow reversal. This wave tailoring is achieved as shown in the schematic of Fig. 1, the key feature being that upon rupture of the diaphragm the flow is geometrically expanded from the apex at the closed end of the driver past the diaphragm station and into a transition section. The consequent wave dynamics are well described by Brode [27,28] and others.

The primary shock wave immediately develops a decaying profile due to the geometric area expansion; furthermore, the flow-field includes an outswep secondary shock embedded in the expanding driver gases, which re-enters the driver and reflects from the apex to re-emerge in the negative phase of the propagated wave. Once the waveform is fully developed

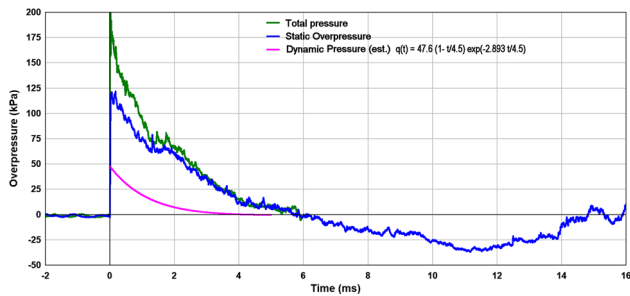


Fig. 2 The standardized incident blast-wave exposure for the current tests showing measured records for static overpressure and total pressure and the derived curve-fit for the dynamic pressure

in the transition section, the flow is gradually re-converged before entering the test section. The wall curvature of the transition has to be minimized to preclude transverse waves and achieve one-dimensional flow by the test section. The rate of area expansion from the driver can be modified by the initial outward curvature of the ABS side walls. Technically that wall curvature should be mildly parabolic-outward to simulate spherical blast, but in practice the simpler straight-wedge design generates waveforms more closely replicating those of actual explosive blast in the regime of 0.5–5 atm overpressure. Further wave-shaping can be achieved by the use of helium as the driver gas but that was not applied in the current work.

An example of the simulated blast waveform used as the standardized exposure in the current work is shown in Fig. 2. The shock waves had an average $M_s = 1.44$ with 125 kPa peak static overpressure and positive duration of 6 ms followed by a negative phase; the shock level corresponds to 47.6 kPa in dynamic pressure and 213 m/s in flow velocity. It is important to note that in an explosive blast wave, the dynamic pressure decays much more abruptly than the static pressure [27]. The ABS is a relatively new technology, and the current variance in profiles is somewhat high, including fluctuations of the order of 8%, due to non-ideal diaphragm rupturing. However, these variances are mostly due to transverse wave perturbations that do not have a strong effect on the net downstream shock wave flow effects, as shown by the positive-phase impulse which varied less than 4%.

The test spheres were fabricated from rigid-plastic shells (Precision Plastic Balls) of approximately 1-mm wall thickness filled with an adhesive foam having various densities (Foam-iT); the filler was further uniformly seeded with metal pellets if necessary to achieve particular densities. Once cured, the ballasted foam fill is very rigid and strong. The spheres are prepared as halves and then carefully glued together with a strong polyurethane adhesive. A small hook was embedded in the top of each sphere to allow its hanging from the inside top of the test section until released for

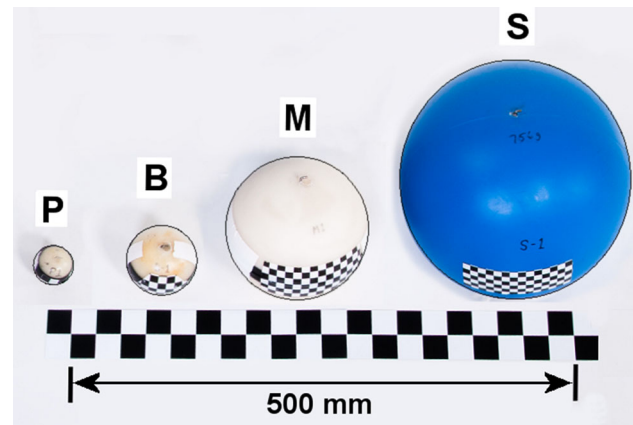


Fig. 3 Test matrix of ball sizes and masses

free-flight motion into the shock wave flow. The test matrix of ball sizes and masses is given in Fig. 3 and Table 1. Different sphere densities, which typically varied by factors of 10, were employed to explore the effect of different acceleration rates for a given sphere size.

It was important that the release mechanism be as free as possible from imparting any force on the ball, which would confuse the analysis of the free-flight motion induced by the shock wave. As depicted in Fig. 4, a simple mechanical swing-release catch of stiff metal wire was devised that was activated by the rupture of the diaphragm at the driver. There was some concern that friction at the catch might induce a small impulsive load at the hanger hook during release. However, any such load at the catch must also impart a moment and therefore a spin on the sphere; therefore, measurement of the spin imparted on the sphere knowing its rotational inertia provides a direct measure of any falsely imparted impulse in the direction of travel that could be factored into a correction for the downstream motion. However, careful tracking of the imaging landmarks on the sphere showed that negligible spin was being imparted, proving that the release mechanism was not causing artifacts that might confuse the motion due to the shock wave flow.

The downstream motion of the sphere was tracked by means of a Phantom 16001 v2011 high-speed video camera at 25,000 frames/s with spatial resolution of 3 pixels/mm. At least two and usually three landmark points were tracked for each sphere, typically the leading and trailing edges at the equator and either the sphere center or top, which were then averaged. Although automated tracking of designated landmarks is possible with most software intended for technical analyses of video imaging, including the Cine Viewer (Cv) application provided with the Phantom by Vision Research, it was found that careful manual tracking using the Cv software provided the most reliable and consistent results.

Table 1 Specifications for sphere sizes and masses

Sphere designation	Diameter (cm)	Volume (cm ³)	X-Area (cm ²)	Mass (g)	Density (g/cm ³)	Areal density (g/cm ²)
P-1	3.85	29.88	11.64	11	0.37	0.94
P-2	3.85	29.88	11.64	36	1.20	3.09
P-3	3.85	29.88	11.64	69	2.31	5.93
P-4	3.85	29.88	11.64	144	4.82	12.37
B-1	6.9	172.0	37.4	52	0.30	1.39
B-2	6.9	172.0	37.4	145	0.84	3.88
B-3	6.9	172.0	37.4	283	1.65	7.57
B-4	6.9	172.0	37.4	572	3.33	15.30
M-1	14.3	1531.	160.6	192	0.13	1.20
M-2	14.3	1531.	160.6	557	0.36	3.47
M-3	14.3	1531.	160.6	1138	0.74	7.09
M-4	14.3	1531.	160.6	2269	1.48	14.13
S-1	25.1	8279.	494.8	765	0.092	1.55
S-2	25.1	8279.	494.8	1910	0.231	3.86
S-3	25.1	8279.	494.8	3685	0.445	7.45
S-4	25.1	8279.	494.8	7937	0.959	16.04

3 Results

As will be discussed later, it follows directly from the drag equation that for the purposes of analyzing downstream motion the relevant fluid-dynamic pressure forces on the sphere surface, of whatever nature, effectively act on the net presented area A_p relevant to the motion direction, in this case $\pi D^2/4$ for sphere diameter D . Similarly, the intrinsic retarding effect on sphere motion will be its mass m . Therefore, scaling of the motion data (x , \dot{x} , or \ddot{x}) by the areal density m/A_p can be expected to factor-out the intrinsic physical parameters of the sphere affecting motion to isolate the effect of the forcing function itself. For example, if the spheres were uniformly accelerated from rest by some manner of quasi-steady drag, we would expect all these scaled displacements to initially exhibit parabolic-type trajectories; the differences between these curves would isolate differences in their respective drag functions, including drag coefficient. The areal-density scaling factor has been used from early studies of blast-induced motion, e.g., [3,29].

Results for tracking of the M-series spheres are shown for illustration in Fig. 5 to the time of 12 ms from shock arrival being twice the duration of the positive phase of the blast wave. The downstream trajectories are shown both unscaled and scaled by areal density; it can be seen that the scaled displacement results collapse effectively onto a single curve. For a given sphere size, this confirms that the downstream motion is imparted by the same loading function and factored only by the sphere mass.

The motion of the M-sized sphere can be seen to have three phases:

1. A distinct initial kickoff velocity imparted in the timescale of the shock-front diffraction over the sphere
2. An immediate *deceleration* phase during the 6-ms period of positive duration
3. Enhanced deceleration after the shock wave positive duration when the sphere is moving through the weak reverse flow of the negative phase.

The motion tracking of this larger sphere was chosen for illustration partly to draw attention to the damped oscillatory behavior evident within the first two milliseconds of response; the fluctuation can be seen as more severe with increasing mass of sphere. This response does not represent the rigid-body motion of the sphere but is in fact a vibration mode of the elastic coupling of the fill with the shell. That is, the light but stiff shell moves abruptly downstream with the incident impulsive shock load, while due to its inertia, the heavy internal fill does not move but is slightly compressed on its upstream side and expanded on the downstream side; the vibration amplitude is very small, being of the order of 0.5 mm. Although the intent of the experiments was to track rigid-body motion, this observation demonstrates that the response of real structures to such loading would include the dynamics of the coupled shell/fill system even if seemingly very rigid. This mode of response dynamics is akin to the coup/contracoup injury of the human skull/brain system [30,31] and relevant to the ultimate interest in resolving how mechanical stresses become imparted to a human head exposed to blast.

After the initial load pulse from the shock diffraction, the motions of shell and fill quickly re-converge to move as a rigid

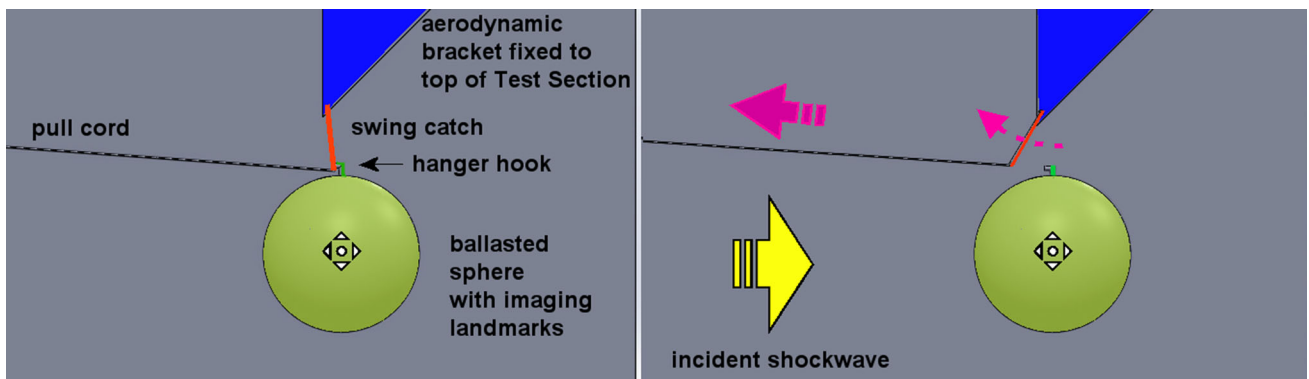


Fig. 4 Sphere release mechanism activated just prior to shock arrival

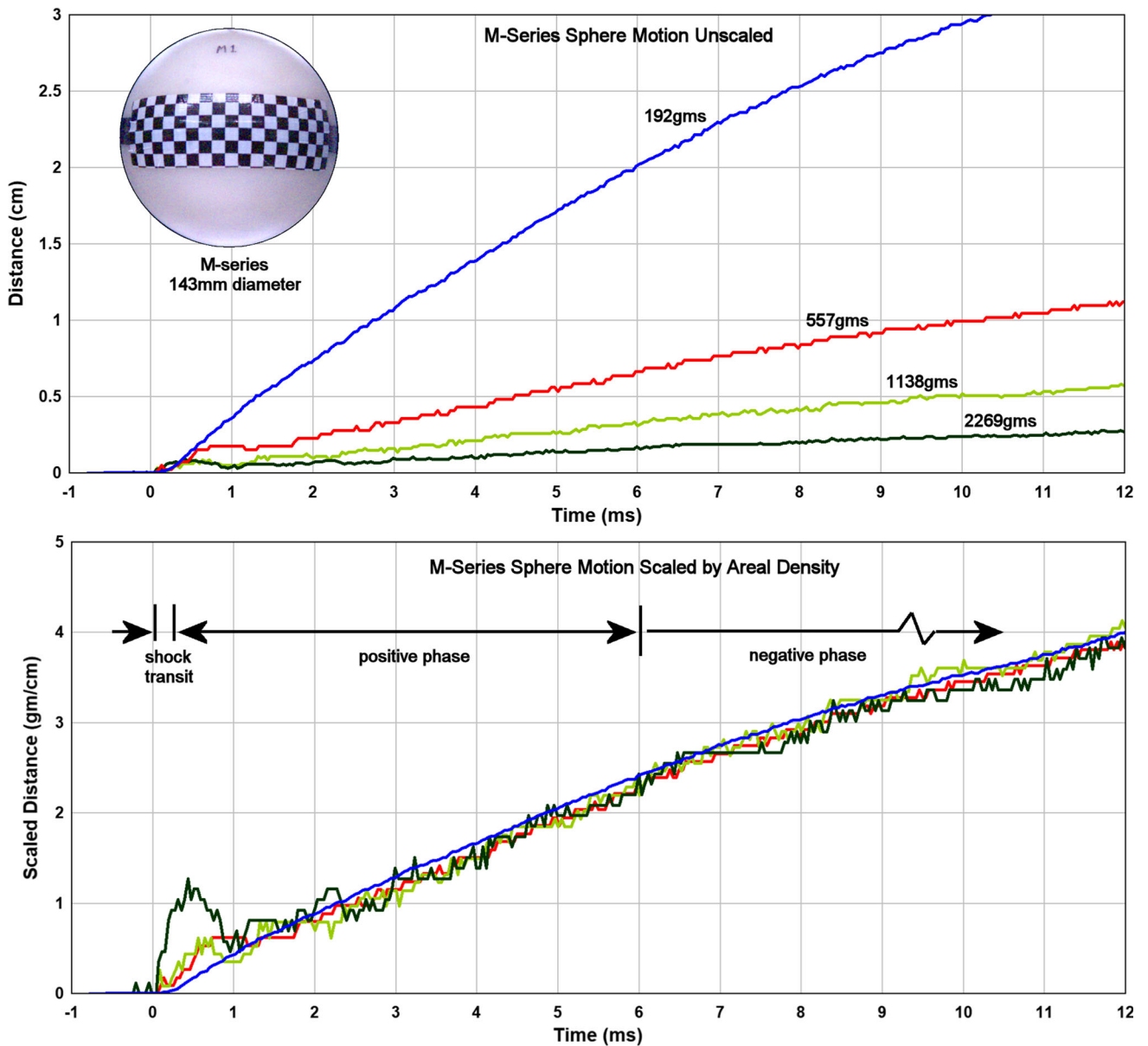


Fig. 5 Downstream motion of the M-series spheres presented unscaled (upper) and scaled by areal density (lower)

body; however, a mild oscillatory response is still evident for the heaviest sphere throughout the tracking of its downstream motion. The compiled graphs of sphere motion for all four sphere sizes as scaled by areal density are given in Fig. 6. The original tracking of the two heaviest of the largest spheres, S3 and S4, was corrupted by the extreme level of the coupled shell/fill response dynamics that in fact damaged the models; new stronger models were required to be fabricated in order to track their rigid-body motion.

The averaged displacement curves scaled by areal density for each sphere size are plotted in Fig. 7, which also includes a graph of these same trajectories normalized to their final displacement at 12 ms. These graphs show a distinct change in the behavior of the motion related to sphere size having factored-out the intrinsic effects of areal density. There is a clear and systematic shift in the nature of the response from drag-dominated for the smaller spheres to diffraction-dominated for the larger. Diffraction-dominated motion begins with an abrupt kickoff velocity imparted by the impulse of the shock-diffraction loading followed by deceleration through the blast-wave flow, which is then enhanced during the negative phase. Drag-dominated motion begins with what appears to be the same kickoff velocity in absolute terms for the same sphere density, as will be discussed later. However, that kickoff velocity is short-lived due to the lower inertia of the smaller spheres and quickly lost in the subsequent acceleration by the positive phase of blast-wave flow. As with the larger spheres, the motion of the smaller spheres falls into deceleration with the negative phase of blast flow as would be expected.

With some important caveats that will be elaborated upon, cubic polynomial curves were fit to the early sphere displacements as scaled by areal density in Fig. 8a from which derivatives for scaled velocity and acceleration are shown in Fig. 8b. Only the first half of the positive phase following shock diffraction has been curve-fit at this time representing the period of primary interest regarding the flow phenomenology. The diffraction phase itself is a different loading process and will be treated here as simply an impulsive event imparting the initial kickoff velocity to the post-diffraction motion. These curve-fits quantify the fundamental differences in motion evident from the displacement records. That is, despite having a very low kickoff velocity relative to the freestream flow, the larger spheres are immediately decelerated; the smaller spheres are also subjected to a kickoff velocity but are then accelerated in to a degree inversely related to size. The simplistic cubic polynomial curve-fit for displacement forces the acceleration function to be linear with time, which is unlikely the case across the full 3-ms sample window considered here. However, acceleration derived in this manner provides a credible estimate of the relative magnitude and rate of change of acceleration between sphere sizes for the middle of the 3-ms sample window.

For the same dataset, different curve-fit functions can yield significantly different results for time derivatives; in fact, a particular function type such as a polynomial will yield different results dependent on the order of polynomial and sample window chosen. The authors would prefer to have first resolved the physics or fluid-dynamics governing the motion from which a properly parameterized mathematical or semi-empirical model for motion might be derived. Applying an otherwise arbitrary curve-fit such as a polynomial can bias results especially in the case of derivatives such as for velocity and acceleration. For example, although a simple cubic polynomial was used for the early post-diffraction motion, there is no reason to think that the acceleration should be linear with time and in fact it is probably exponential-like for very small spheres. Therefore, the results from polynomial curve-fits to the post-diffraction motion are presented here for expediency at this time to provide best-available estimates for velocity and acceleration for the prescribed time-window.

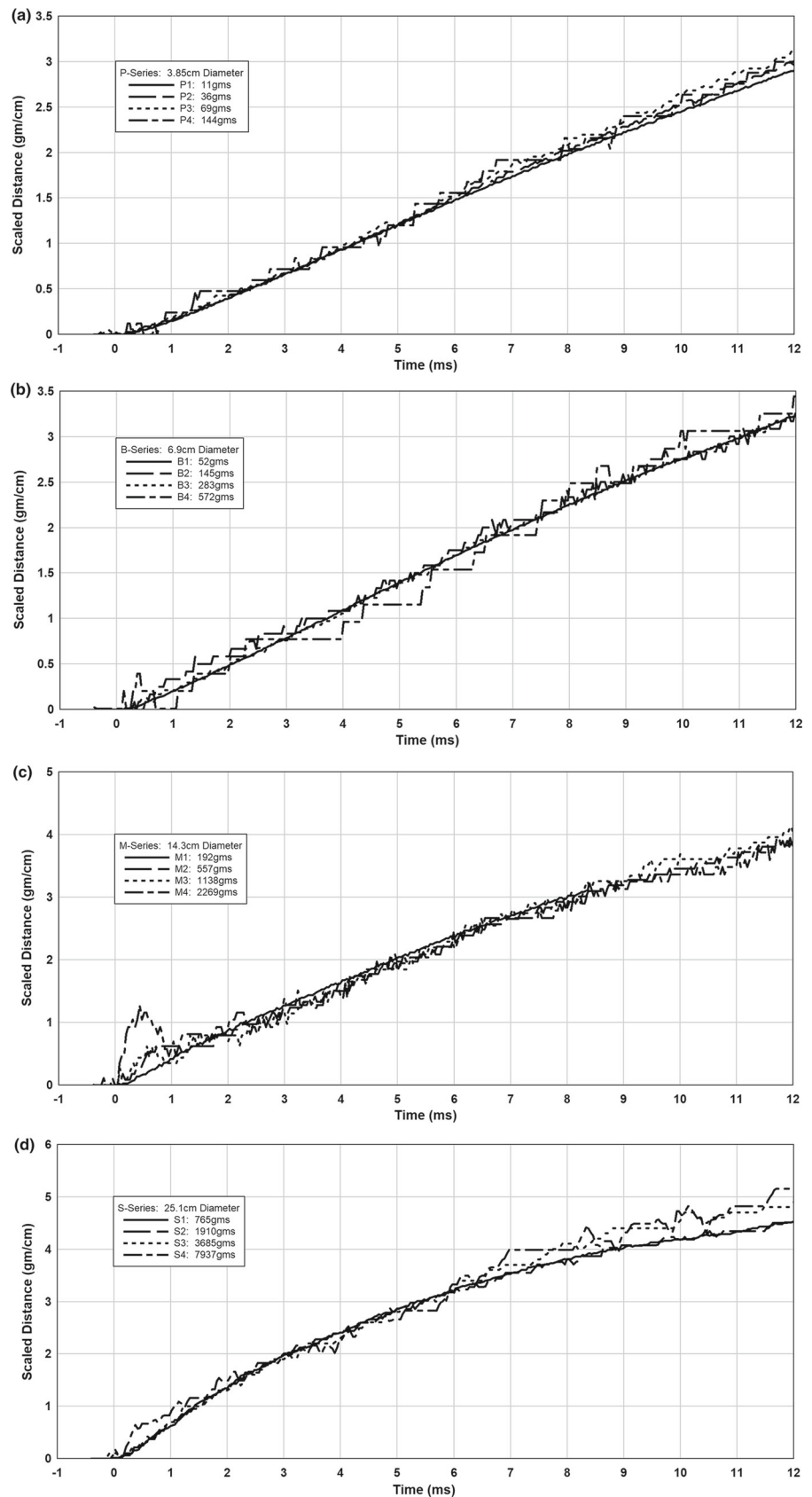
The data suggest that for the currently simulated blast-wave condition, there is a sphere size of perhaps 8 cm diameter that would experience steady motion in the early post-diffraction flow preserving its kickoff velocity. Coincidentally, 8 cm is the sphere size studied in the experiments of Sun et al. and Tanno et al. using a vertical shock tube [9, 11, 13]. However, those experiments were restricted to the duration of the diffraction phase for a step-function shock wave and did not allow analyses of motion in the post-diffraction flow which is of particular interest here.

It is important to recall that all trajectories above have been scaled by areal density as a means to show the different nature of sphere motion as a function of size on the same graph with the intrinsic effects of mass and presented area factored-out. It is possible to extract the kickoff velocity for each sphere size, being the initial slope of the post-diffraction displacement record, as determined from these curve-fits and furthermore estimate the absolute kickoff velocity scaled only by sphere density, as shown in Fig. 8c. The error bounds shown in the figure are somewhat subjective in that the estimated velocity is a function of not only the experimental data but also the choice of curve-fit. Within the bounds of the current experimental error and the effects of curve-fit technique, the consolidated data for the four sphere sizes with wide-ranging densities suggest that the kickoff velocity is nearly constant for any sphere size having the same density.

4 Discussion

By classical analyses there are potentially four types of fluid-dynamic forces affecting the motion of objects in this kind of flow condition:

Fig. 6 Sphere displacement scaled by areal density; **a** P-series; **b** B-series; **c** M-series; and **d** S-series



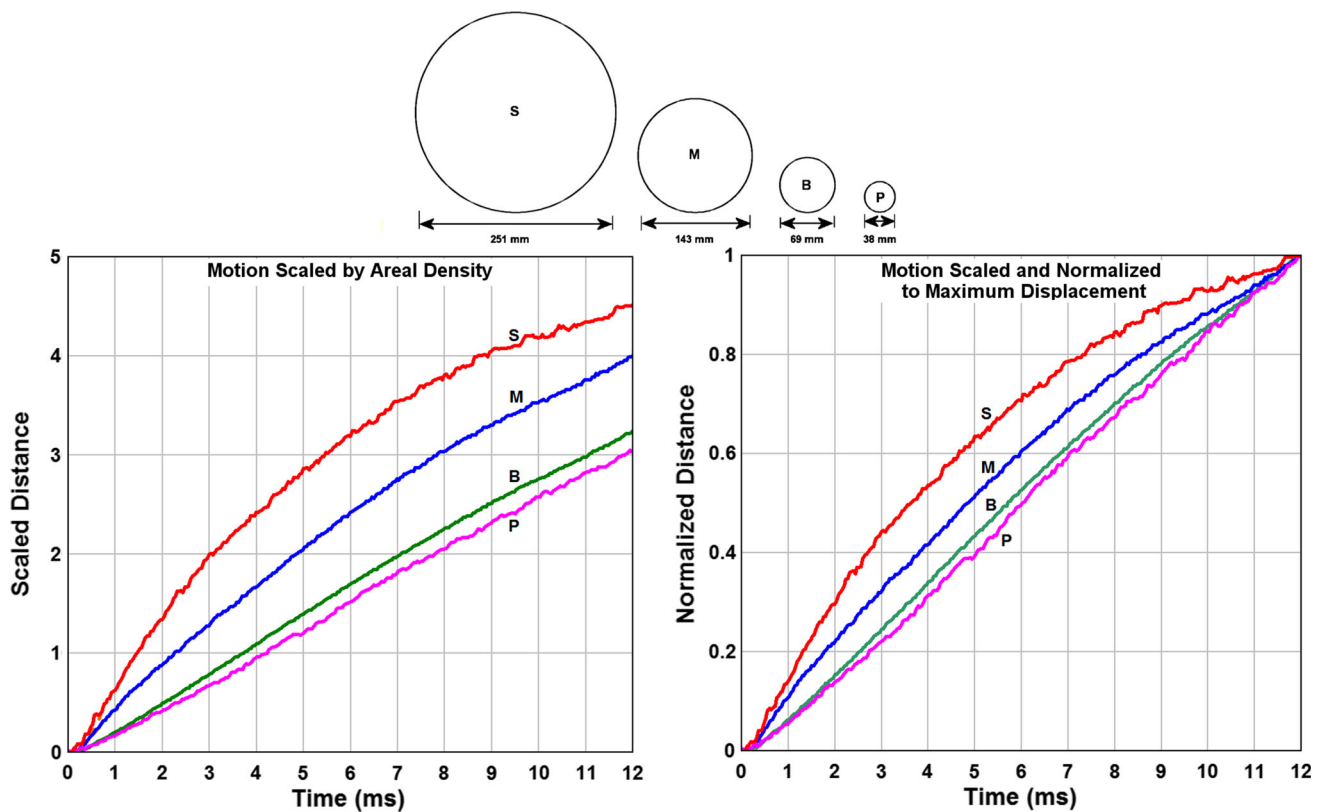


Fig. 7 Graphs of the average scaled motion for each sphere size showing the change in response from drag-dominated to diffraction-dominated with increasing sphere size. The graph at right presents the

same displacement data normalized to the displacement at 12 ms to highlight the differences in acceleration as shown by their relative curvatures

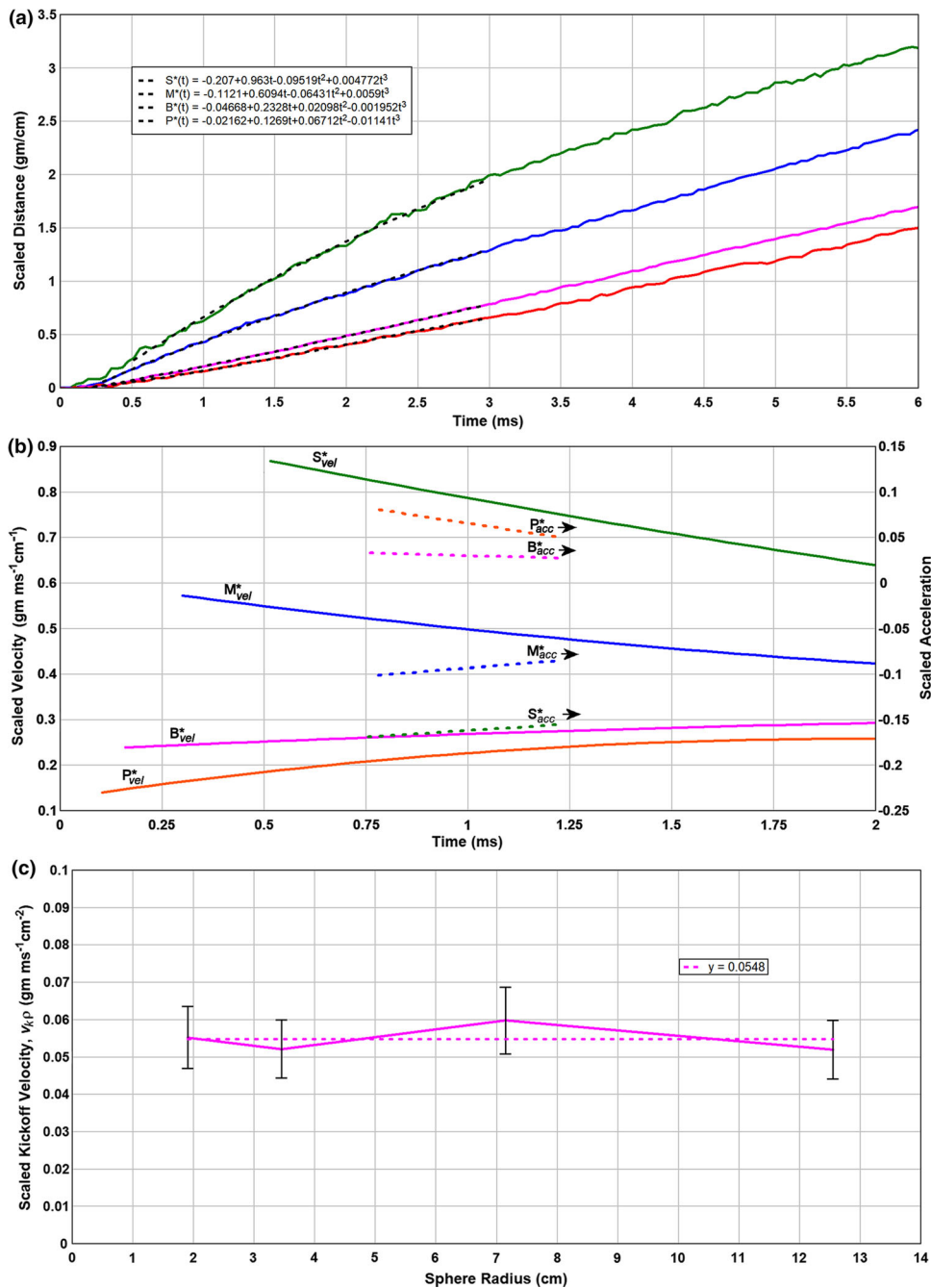
1. Shock wave loading during the diffraction phase
2. Drag loading during the shock wave after-flow (or “blast wind”) comprising both viscous (skin friction) and form (pressure distribution around the body) components
3. Basset force (rate of change of momentum of the boundary layer)
4. Added mass effect (proportional in this case to half the mass of the volume of air displaced by the sphere).

Reference [8] showed that for the regime of sphere sizes and masses relevant here (3) and (4) can be neglected, and in their case diffraction could also be neglected. The objective of the current study is to resolve the roles of (1) and (2) for the particular problem of a rapidly decaying shock wave flow characteristic of blast waves relevant to IED-scale attacks. The incident shock wave flow falls to reverse-flow conditions during the time frame when such spheres would still be accelerating in the case of a step-function shock wave with steady after-flow. The fact that diffraction-induced motion must dominate for certain blast-wave conditions is clear if one considers the extreme case where the blast wavelength λ approaches that of the characteristic length of the structure such as the sphere diameter D . In such a case, there is effectively no blast wind after-flow over the structure, and hence no prospect for development of true drag-force action.

Substantial work has been conducted on (1) for the case of a step-function shock wave with steady after-flow with very consistent results from both experimenters and modelers. As shown in [9] for a given incident step shock wave, the duration of the diffraction loading waveform scales very well with sphere diameter; extracts from a key figure in that paper are reproduced in Fig. 9. These results from [9] were also independently corroborated by computational studies described in [12] comparing results from three commercial hydrocodes. Since the amplitude of the diffraction force–time function scales as D^2 and its duration scales with D , it can be deduced that the imparted impulse from shock diffraction, being the area under the force–time curve, is scalable and proportional to D^3 . Since the sphere mass also scales with D^3 , this implies the kickoff velocity from the shock-diffraction impulse will be constant for any sphere size of the same density. This deduction regarding the expected kickoff velocity based on the computational study of [9] is supported by the current results presented in Fig. 8c.

In the current study, the shock wave flow is rapidly decaying, unlike a step-function wave. Therefore, considering the shock-transit time of about 0.5 ms for the largest S-series sphere, the freestream shock after-flow conditions have decayed nearly 25% in static overpressure and 35%

Fig. 8 **a** Cubic polynomial curve-fits to the early post-diffraction motion to 3 ms; **b** scaled velocity and acceleration for the early post-diffraction motion as determined from the curve-fits; and **c** kickoff velocity from the diffraction impulse loading as scaled by sphere density only



for dynamic pressure during the shock diffraction; therefore, the kickoff velocity would be expected to be somewhat low for that case compared to the result expected from [9]. Another factor which bears consideration but has not yet been quantified is the “real-world” effect of material shock transmission and structural deformation modes of the spheres themselves, particularly the larger spheres. Such material response dynamics are ultimately energy-absorbing mechanisms that would detract from the theoretical results for true rigid-body motion of a sphere in a step-function shock wave flow as predicted by [9].

In the current study the incident blast-wave simulation was kept constant for the experiments; hence, the variation of the amplitude of the diffraction load function with shock strength was not a consideration. However, the authors propose that this amplitude likely scales with that of the normally reflected shock, which seems supported by results presented in [10].

Moving on to the matter of the post-diffraction flow, the prevailing analyses for shock-wave induced motion dominated by drag presume an unsteady variant of drag as defined in classical aerodynamics, i.e.,

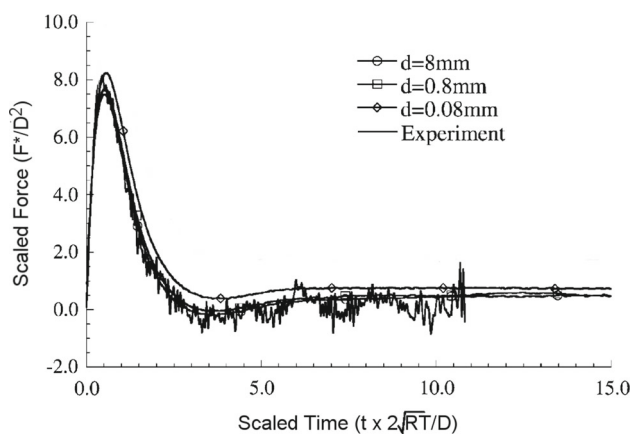


Fig. 9 The shape of the diffraction-phase loading function from a step-function shock wave, $M_s = 1.22$, over various sphere sizes and as experimentally determined for an 80-mm sphere (from Sun et al. [9])

$$F_d = C_d S (1/\rho v_r^2), \text{ where}$$

F_d drag force

C_d (unsteady) drag coefficient; C_d is a function of Reynolds Number, $Re = \rho V_r D / \mu$, where μ is the dynamic viscosity of the air

S presented area, $\pi D^2/4$, for sphere diameter D

ρ gas density

v_r relative flow velocity between sphere and air

Note that all the gasdynamic conditions refer to the shock wave values that are decaying rapidly during the course of the motion in the current study. The peak Reynolds number at the shock front is approximately $22 \times 10^6/m$.

The premise for aerodynamic drag loading is that the flow forces are entirely based on the kinetic energy of the free-stream flow as defined by the dynamic pressure $1/2\rho v^2$; there is no consideration of the role of gradients in the freestream static pressure. Furthermore, the flow patterns are presumed to be of a particular type for a given Re such as laminar Stokes flow at very low Re . In reality, the gradients in freestream static pressure, particularly at the shock front itself, dominate the diffraction loading, and artifacts of the diffraction phase such as possible large-scale vortex structures may persist long after the shock passage. In the current case, the shock-front flow velocity is 213 m/s with $Re \sim 22 \times 10^6$ per meter, yet Re decays to zero within 6 ms followed by flow reversal in the negative phase. It is improbable in the case of such a short-duration blast interaction with objects that flow artifacts of the diffraction phase and early high-speed flow including vortex development, zones of different entropy, and turbulence simply disappear within 6 ms once the freestream flow has decayed, as would be assumed in quasi-steady analyses.

The deceleration of the larger spheres following their kick-off velocity during the period of the positive phase as shown in Figs. 6, 7, and 8 merits discussion since by standard quasi-steady flow assumptions this implies that the larger spheres have a negative drag coefficient. The highest kickoff velocity imparted by diffraction is less than 6 m/s developed in about 0.5 ms for the lightest S-sphere during the shock diffraction. Although the shock wave is decaying, these spheres are still within very high-speed freestream flow having initial velocity exceeding 200 m/s. The flaw with interpreting this result as inferring a negative drag coefficient relates to the assumption that the flow pattern at a particular time after diffraction resembles that of a steady flow at that particular freestream dynamic pressure.

Although the authors were expecting different motion behavior for the larger spheres, the evidence of a powerful upstream force on the spheres in the post-diffraction flow was entirely unexpected. The flow-diagnostic resources and time available for the initial study to simply track sphere motion did not allow proper resolution of this phenomenon. The deceleration effect is unmistakable and repeatable as well as being part of a consistent pattern of behavior from the smaller to larger spheres. As an expedient diagnostic, flow-tracer material was applied to the upper surface of the larger spheres. A plausible hypothesis for the deceleration is evident from subsequent flow visualization tests as shown in Fig. 10. These supplemental tests show that a large and strong ring vortex develops in the zone at the back of the sphere; the vortex persists at the backside of the sphere for the entire duration of the tracking as shown in Fig. 10 and in fact moves upstream toward the front of the sphere during the negative phase of flow velocity before dissipating. Such a vortex would be promptly shed downstream in the case of the steady after-flow of a step-function shock wave but stays attached to the backside of the sphere in the case of a decaying wave due to the adverse gradients in the freestream flow. The ring vortex would induce a localized counter-flow on the back of the sphere, which retains high speed despite the decay of the freestream flow. This flow structure may also behave as a form of added mass to downstream motion since the surface streamline becomes separated from the sphere and envelops this vortex system.

Development of vortices in the afterbody region of an object from the shock-diffraction process is well known from early blast/target studies, e.g., [32]. Such a vortex is also predicted from CFD calculations for blast flow over targets although by somewhat different mechanisms for viscous and inviscid flows, e.g., [18]. Although Ofengeim and Drikakis [18] considered the case of blast-wave interaction with a cylinder rather than a sphere, similar basic phenomenology can be expected. That study shows that a significant vortex is not developed if the blast wavelength is too short relative to the cylinder diameter and that the vortex would be shed

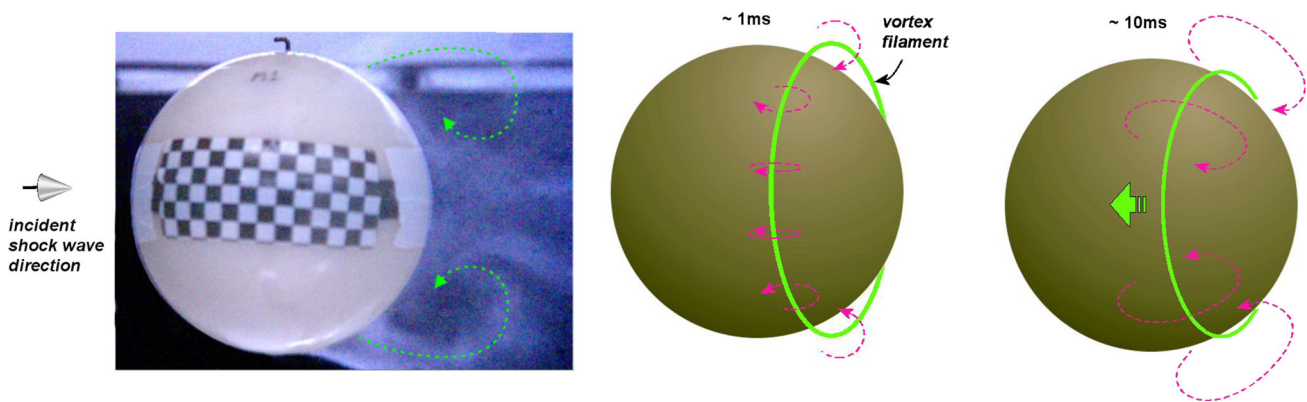


Fig. 10 Flow visualization of the larger spheres showing the development and persistence of a ring vortex on the downstream side



Fig. 11 Visualization of the blast-wave flow around a replica skull head-form at 1.0 and 5.7 (onset of negative phase) and 8 ms after shock arrival

if the blast wavelength is very long or a step function. They drew attention to this vortex staying close to the back of the cylinder in the case of a decaying blast wave. This suggests there is a regime of blast wavelength to sphere diameter as in the current study that will allow the development of a strong afterbody vortex that will not be shed. The effect of a ring vortex on sphere loading in the case of the blast/sphere interaction will be substantially stronger than the same phenomena in the case of the cylinder.

A replica human skull head-form was tested in the face-on orientation using the same experimental setup as shown in Fig. 11. Measurements were taken of both the flow patterns developed around the head-form using particle tracers as well as tracking of free-flight motion. The cranium was ballasted by means of a tightly fitting water-filled bag, while the sinus and orbits were blocked with modeling clay. However, as shown no attempt was made to account for skin, hair, or musculature. This experiment was intended only to add incrementally to the understanding of phenomena relevant to blast-induced motion in the case of the human head.

As shown in Fig. 11, an irregular and relatively weak vortex was developed on the backside of the skull; the uniformity and strength of the ring vortex in the case of a sphere relates to its axisymmetry and surface smoothness. However, both the basic flow pattern and global motion of the head-form show important similarities to results for comparably sized spheres, particularly with regard to the abrupt but low kick-off velocity followed by deceleration. Based on volume, the

M-sphere is a very close match for the adult human cranium ($\sim 1250 \text{ cm}^3$). However, the shape of the entire skull affects the flow-field interaction; the curvature of the skull-replica forehead best matches the M-series; the S-series best matches the skull top. The skull face being somewhat flat causes the shock wave flow around the head to differ from that of the sphere.

The skull motion has not been analyzed fully at this time but clearly includes both linear and rotational action. For a sphere of uniform density, the center of pressure for the blast load is the same as the center of mass; hence, a rotational moment should not be imparted. For the skull, the center of mass is very near the centroid of the cranium and higher than the center of frontal pressure loading, which is relatively low due to the effect of the somewhat flat face and mandible. Therefore, a significant rotation that is clockwise in the view of Fig. 11 is imparted by the blast. As with the linear acceleration, the rotational moment seems primarily imparted as an impulse during the shock reflection and diffraction rather than by quasi-steady aerodynamic drag.

There are two quite different paths forward from this initial exploratory investigation. With regard to the blast-induced rigid-body motion of inert spheres, a more rigorous experimental study is required to properly resolve the post-diffraction flow phenomena causing the systematic change of motion as a function of sphere size. Such a study would ideally employ shock-flow imaging techniques and instrumentation to resolve the details of the flow velocity and

pressure, particularly in the after-body region. As originally intended, CFD modeling will also be applied to resolve the shock diffraction and vortex formation accounting for viscous phenomena such as boundary layer behavior and turbulence. However, the large scale of vortex observed using the current flow-tracer method suggests that an inviscid flow simulation might reveal certain important flow structures as suggested from [18].

With regard to the task of understanding the mechanisms by which stress is imparted to the human brain from blast exposure and how this might be mitigated, a different approach and design of test sphere are required. Rather than investigating rigid-body motion with focus on the external shock wave flow dynamics as above, it would be required to use a spherical shell and fill that are structurally responsive as in the case of the human skull/brain system. Such a test sphere would comprise a stiff but elastic shell and fluid-like fill including embedded strain gauges to assess the material and structural response dynamics, particularly during the shock diffraction and early impulsive motion. Measurements of the internally imparted stress for this responding shell/fill system would allow assessments of the efficacy of shielding systems such as improved helmet design as well as the effect of relevant real-world boundary conditions such as the head articulation with a responding neck or neck/torso model. Use of a simple spherical shell facilitates understanding of the basic mechanisms governing the imparted stresses and allows validation of computational modeling. Subsequent to understanding effects for the simple spherical analogue, it is feasible to add complexities of a more biofidelic physical model having realistic skull geometry and simulated tissues.

5 Conclusion

An experimental study has been completed to investigate scaling effects relevant to blast-induced rigid-body motion of spheres where the sphere sizes and masses were varied for a particular blast-wave exposure. The standardized test condition was a blast wave of 125 kPa amplitude with 6-ms positive-phase duration followed by a negative phase in both static overpressure and flow velocity. The sphere sizes spanned the regime where the acceleration was drag-dominated to diffraction-dominated. Diffraction loading in this case is characterized by an abrupt but relatively low-amplitude kickoff velocity imparted during the very short timescale of the shock passage over the object; there is in fact greatly diminished air flow around the sphere during this process, hence minimal aerodynamic drag. Drag-dominated response is characterized by a quasi-steady acceleration due to the dynamic pressure of the shock wave after-flow.

The smallest spheres tested were 38.5 mm in diameter and responded with a very minor degree of initial kickoff

velocity followed by weak acceleration during the positive phase evolving to deceleration during the negative phase. The response of the largest spheres of 251 mm diameter was dominated by impulsive but low-level motion from the diffraction, followed by two stages of deceleration. Expedient flow visualization showed that the deceleration of the large spheres was likely related to the persistence of a strong ring vortex on the downstream side of the sphere. The results have implications for the design and interpretation of blast-induced acceleration injury to personnel and scaling of model experiments. Further investigation is required to confirm motion scaling effects as a function of blast amplitude and wavelength as well as to resolve how the shock-wave induced flow patterns in a decaying wave affect the sphere motion.

Acknowledgements Funding was provided by the US Army Medical Research and Materiel Command through the Congressionally-Directed Medical Research Programs (Award No. W81XWH-12-2-0127).

Disclaimer Material has been reviewed by the Walter Reed Army Institute of Research. There is no objection to its presentation and/or publication. The opinions or assertions contained herein are the private views of the author and are not to be construed as official, or as reflecting true views of the Department of the Army or the Department of Defense.

References

1. Bryant, E.J., Allen, F.J.: Dynamic pressure impulse for near-ideal and non-ideal blast waves—height of burst charts. Kaman Tempo, KT-81-014(R), Santa Barbara, CA 93102, (DNA Contract Report DNA-5826F) (1981)
2. Lee, C.K.B., Summa, W.J., Urban, J., Pfeffer, R.A.: A simple correlation between dynamic pressure impulse and vehicle velocity. In: 16th Symposium on Military Applications of Blast and Shock (MABS16), Oxford, UK (2000)
3. Ethridge, N., Flory, R.A.: Use of cube displacements as a measure of airblast. In: 13th Symposium on Military Application of Blast Simulation (MABS13), The Hague, The Netherlands (1993)
4. Igra, O., Ben-Dor, G.: Dusty shock waves. *Appl. Mech. Rev.* **41**, 379–437 (1988). doi:[10.1115/1.3151872](https://doi.org/10.1115/1.3151872)
5. Gallagher, E.V.: Air blast loading on arches and domes. Final Test Report No. 13, Armour Research Foundation of Illinois Institute of Technology (1958)
6. Mellisen, S.B.: Airblast loading of spherical radomes. In: Proceedings of 2nd Military Applications of Blast Simulators, MABS2, Naval Weapons Laboratory, Dahlgren, VA (1970)
7. Jourdan, G., Houas, L., Igra, O., Estivaleres, J.-L., Devals, C., Meshkov, E.E.: Drag coefficient of a sphere in a non-stationary flow: new results. *Proc. R. Soc. A* **463**, 3323–3345 (2007). doi:[10.1098/rspa.2007.0058](https://doi.org/10.1098/rspa.2007.0058)
8. Igra, D., Igra, O., Houas, L., Jourdan, G.: Simulation of sphere's motion induced by shock waves. *J. Fluids Eng. Trans. ASME* **134**(10), 104502 (2012). doi:[10.1115/1.4007385](https://doi.org/10.1115/1.4007385)
9. Sun, M., Saito, T., Takayama, K., Tanno, H.: Unsteady drag on a sphere by shock wave loading. *Shock Waves* **14**, 3–9 (2005). doi:[10.1007/s00193-004-0235-4](https://doi.org/10.1007/s00193-004-0235-4)
10. Skews, B.W., Bredin, M.S., Efun, M.: Drag measurement in unsteady compressible flow, Part 2: Shock wave loading of spheres and cones. *R&D J. South Afr. Inst. Mech. Eng.* **23**(1), 13–19 (2007)

11. Tanno, H., Itho, K., Saito, T., Abe, A., Takayama, K.: Interaction of shock with a sphere suspended in a vertical shock tube. *Shock Waves* **13**, 191–200 (2003). doi:[10.1007/s00193-003-0209-y](https://doi.org/10.1007/s00193-003-0209-y)
12. Schwer, L.: Air shock driven fluid–structure interaction: Verification and validation considerations. In: *Military Aspects of Blast & Shock (MABS22)*, Bourges, France (2012)
13. Tanno, H., Komuro, T., Takahashi, M., Takayama, K., Ojima, H., Onaya, S.: Unsteady force measurement technique in shock tubes. *Rev. Sci. Instrum.* **75**(2), 035107 (2004). doi:[10.1063/1.1641156](https://doi.org/10.1063/1.1641156)
14. Zhang, L.T., Wang, T.H., Hao, L.N., Huang, B.Q., Chen, W.J., Shi, H.H.: Experimental investigation of shock wave diffraction over a single- or double-sphere model. *Shock Waves* **27**(1), 97–107 (2017). doi:[10.1007/s00193-016-0641-4](https://doi.org/10.1007/s00193-016-0641-4)
15. Britan, A., Elperin, T., Igra, O., Jiang, J.P.: Acceleration of a sphere behind planar shock waves. *Exp. Fluids* **20**, 84–90 (1995). doi:[10.1007/BF00189297](https://doi.org/10.1007/BF00189297)
16. Igra, O., Takayama, K.: Shock tube study of the drag coefficient of a sphere in a non-stationary flow. *Proc. R. Soc. A* **442**, 231–247 (1993). doi:[10.1098/rspa.1993.0102](https://doi.org/10.1098/rspa.1993.0102)
17. Parmar, M., Haselbacher, A., Balachandar, S.: Modeling of the unsteady force for shock–particle interaction. *Shock Waves* **19**, 317–329 (2009). doi:[10.1007/s00193-009-0206-x](https://doi.org/10.1007/s00193-009-0206-x)
18. Ofengeim, D.Kh., Drikakis, D.: Simulation of blast wave propagation over a cylinder. *Shock Waves* **7**, 305–317 (1997). doi:[10.1007/s001930050085](https://doi.org/10.1007/s001930050085)
19. Temkin, S., Mehta, H.K.: Droplet drag in an accelerating and decelerating flow. *J. Fluid Mech.* **116**, 297–313 (1982). doi:[10.1017/S0022112082000470](https://doi.org/10.1017/S0022112082000470)
20. Temkin, S., Kim, S.S.: Droplet motion induced by weak shock waves. *J. Fluid Mech.* **96**(1), 133–157 (1980). doi:[10.1017/S0022112080002054](https://doi.org/10.1017/S0022112080002054)
21. Goldstein, L.E., Fisher, A.M., Tagge, C.A., Zhang, X.L., Velisek, L., Sullivan, J.A., Upreti, C., Kracht, J.M., Ericsson, M., Wojnarowicz, M.W., Goletiani, C.J., Maglakelidze, G.M., Casey, N., Moncaster, J.A., Minaeva, O., Moir, R.D., Nowinski, C.J., Stern, R.A., Cantu, R.C., Geiling, J., Blusztajn, J.K., Wolozin, B.L., Ikezu, T., Stein, T.D., Budson, A.E., Kowall, N.W., Chargin, D., Sharon, A., Saman, S., Hall, G.F., Moss, W.C., Cleveland, R.O., Tanzi, R.E., Stanton, P.K., McKee, A.C.: Chronic traumatic encephalopathy in blast-exposed military veterans and a blast neurotrauma mouse model. *Sci. Transl. Med.* **4**(134), 134ra60 (2012). doi:[10.1126/scitranslmed.3003716](https://doi.org/10.1126/scitranslmed.3003716)
22. Gullotti, D.M., Beamer, M., Panzer, M.B., Chen, Y.C., Patel, T.P., Yu, A., Jaumard, N., Winkelstein, B., Bass, C.R., Morrison, B., Meaney, D.F.: Significant head accelerations can influence immediate neurological impairments in a murine model of blast-induced traumatic brain injury. *J. Biomech. Eng.* **136**(9), 091004-1 (2014). doi:[10.1115/1.4027873](https://doi.org/10.1115/1.4027873)
23. Josey, T., Sawyer, T.W., Ritzel, D.V., Donahue, L.: High fidelity simulation of free-field blast loading: the importance of dynamic pressure. In: *Personal Armour Systems Symposium (PASS2016)*, Amsterdam, The Netherlands (2016)
24. Ganpule, S., Alai, A., Plougonven, E., Chandra, N.: Mechanics of blast loading on the head models in the study of traumatic brain injury using experimental and computational approaches. *Biomech. Model. Mechanobiol.* **12**(3), 511–531 (2013). doi:[10.1007/s10237-012-0421-8](https://doi.org/10.1007/s10237-012-0421-8)
25. Carneal, C., Merkle, A., Zinn, D., Andrist, J., Clark, J., Alphonse, V., Ritzel, D., Carboni, M., DeChristifano, B., Cyganik, J., Maffeo, M.: Development of a laboratory shock tube system for helmet blast overpressure performance assessment. In: *Personal Armour Systems Symposium (PASS2016)*, Amsterdam NL (2016)
26. Ritzel, D.V., Parks, S.: Shock tube apparatus for blast wave simulation. US Patent 9027383 (2015)
27. Brode, H.L.: Blast wave from a spherical charge. *Phys. Fluids* **2**(2), 217–229 (1959). doi:[10.1063/1.1705911](https://doi.org/10.1063/1.1705911)
28. Brode, H.L.: Numerical solutions of spherical blast waves. RM-1363-AEC, Rand Corporation (1954)
29. Bowen, I.G., Albright, R.W., Fletcher, E.R., White, C.S.: A model designed to predict the motion of objects translated by classical blast waves. CEX-58.9, Civil Effects Study, US Atomic Energy Commission (1961)
30. Shaw, N.A.: The neurophysiology of concussion. *Prog. Neurobiol.* **67**(4), 281–344 (2002). doi:[10.1016/S0301-0082\(02\)00018-7](https://doi.org/10.1016/S0301-0082(02)00018-7)
31. Finger, S.: *Origins of Neuroscience: A History of Explorations into Brain Function*, pp. 429–430. Oxford University Press, Oxford (2001)
32. Glasstone, S., Dolan, P.J. (Eds.): *The Effects of Nuclear Weapons*, 3rd edn. US Dept of Defense and Energy Research and Development Agency (1977)